Electrophysiological characterization of the archaeal transporter NCX_Mj using solid supported membrane technology

Maria Barthmes,[1,2] Jun Liao,[3,5] Youxing Jiang,[3,4] Andrea Brüggemann,[1] and Christian Wahl-Schott[2]

[1]Nanion Technologies, 80636 Munich, Germany
[2]Center for Integrated Protein Science (CIPS-M) and Center for Drug Research, Department of Pharmacology, Ludwig Maximilians University and DZHK (German Center for Cardiovascular Research), partner site Munich Heart Alliance, 81377 Munich, Germany
[3]Department of Physiology and [4]Howard Hughes Medical Institute, University of Texas Southwestern Medical Center, Dallas, TX 75390
[5]School of Life Science and Technology, Shanghai Tech University, Shanghai 201210, China

Sodium–calcium exchangers (NCXs) are membrane transporters that play an important role in Ca^{2+} homeostasis and Ca^{2+} signaling. The recent crystal structure of NCX_Mj, a member of the NCX family from the archaebacterium *Methanococcus jannaschii*, provided insight into the atomistic details of sodium–calcium exchange. Here, we extend these findings by providing detailed functional data on purified NCX_Mj using solid supported membrane (SSM)–based electrophysiology, a powerful but unexploited tool for functional studies of electrogenic transporter proteins. We show that NCX_Mj is highly selective for Na^+, whereas Ca^{2+} can be replaced by Mg^{2+} and Sr^{2+} and that NCX_Mj can be inhibited by divalent ions, particularly Cd^{2+}. By directly comparing the apparent affinities of Na^+ and Ca^{2+} for NCX_Mj with those for human NCX1, we show excellent agreement, indicating a strong functional similarity between NCX_Mj and its eukaryotic isoforms. We also provide detailed instructions to facilitate the adaption of this method to other electrogenic transporter proteins. Our findings demonstrate that NCX_Mj can serve as a model for the NCX family and highlight several possible applications for SSM-based electrophysiology.

The Journal of General Physiology

INTRODUCTION

The cellular transport of ions and biological solutes, such as amino acids, proteins, nucleotides, and carbohydrates, across biological membranes requires specific transport proteins. Aside from ion channels, these proteins can be divided into two main classes: ATP-driven transporters (ABC transporters and P-type and F-type ATPases) and secondary active transporters. The solute carriers (SLCs) represent a major family of the class of secondary active transporters. This group of transporters is very heterogeneous and makes up the second largest group of membrane proteins after the G protein–coupled receptors (Alexander et al., 2013). Functional characterization of these transporters and pumps is often challenging because of the shortage of suitable methods that can provide scientific flexibility and are easily applicable. Binding experiments or flux measurements of fluorescently labeled or radiolabeled substrates in living cells, membrane vesicles, or liposomes are commonly used to functionally characterize transport processes. These techniques allow the direct observation of the substrate flux. The major drawback of these methods is that suitably labeled, preferably nontoxic, substrates are required. Alternatively, transport processes, which include the net transfer of electrical charge (electrogenic transport), can be characterized by electrophysiological methods. The advantage of these methods is that electrical signals, such as transport currents or transport-dependent voltage changes, can be measured without markers and in real time. The conventional patch clamp of native or cultured cells can be used only when the transporters and exchangers of interest display high turnover rates, comparable with those of ion channels (DeFelice and Goswami, 2007). When the current amplitudes of transporters that are recorded in mammalian cells are below the detection limit, *Xenopus laevis* oocytes are often used as an expression system, and whole cell currents are recorded using a two-electrode voltage clamp. The advantage of this method is that oocytes are much larger (~1 mm), and therefore the recorded currents are usually considerably higher in amplitude than the currents recorded from mammalian cells. Several isoforms of the sodium–calcium exchanger (NCX) and other transporters, such as Na^+-coupled glutamate transporters (Wadiche and Kavanaugh, 1998), carbohydrate transporters (SGLTs; Wright et al., 2011), and monoamine

Correspondence to Christian Wahl-Schott: christian.wahl@cup.uni-muenchen.de
Abbreviations used in this paper: GUV, giant unilamellar vesicle; ITO, indium-tin-oxide; NCX, sodium–calcium exchanger; SSM, solid supported membrane.

The Rockefeller University Press $30.00
J. Gen. Physiol. 2016 Vol. 147 No. 6 485–496
www.jgp.org/cgi/doi/10.1085/jgp.201611587

transporters (Henry et al., 2011), have been characterized using these approaches.

However, a major drawback of this method is that the turnover rates of transport proteins are frequently too small for straightforward patch-clamp or voltage-clamp measurements. These techniques might also be precluded or impeded when the analyzed transporters are from intracellular or noneukaryotic membranes. One solution to this problem is to purify transport proteins from bacterial or intracellular membranes and to incorporate them into artificial bilayers. This approach has been successfully applied to a variety of ion channels (Holden et al., 2006; Syeda et al., 2014) and to some transporters, such as the bacterial multidrug transporter LmrA (Velamakanni et al., 2009). Such studies provided valuable information about the membrane biophysics of these proteins. However, one significant disadvantage of self-supported artificial bilayers is that they are limited by size to the micrometer range. Any sizes larger than this often lead to instability and collapse of the bilayer. Therefore, only a restricted amount of protein can be incorporated into the lipid bilayer, substantially limiting the method if the protein of interest has only a low turnover rate, as is the case for many SLC proteins, pumps, and ABC transporters.

A very promising but unexploited alternative approach to measure transporter currents is solid supported membrane (SSM)–based electrophysiology. SSMs consist of an artificial lipid monolayer on top of an alkanethiol monolayer, which is covalently bound to a gold-coated glass plate (Fig. 1). For the electrophysiological measurement of membrane transporters, native membrane fragments or liposomes containing the transporter protein of interest are immobilized on top of the SSM. Synchronous activation of the transport proteins is usually performed by rapid application of a substrate-containing buffer via a perfusion system. The transport current into the vesicles or liposomes can be electrically recorded on the gold surface. The details of the read-out technique are displayed in Fig. 1 (D and E).

A remarkable advantage of the method is that the SSM is not subjected to the size limitation that is common in bilayer experiments. In fact, the area of the SSM can be increased to a diameter of several millimeters, which permits the immobilization of a very large number of liposomes or membrane vesicles on the SSM. The resulting high number of transporter proteins generates a combined electrical current in the order of several hundred picoamperes to nanoamperes, which can be conveniently recorded with an electrophysiological amplifier. In this way, the amplification is sufficient to detect very low turnover rates. Importantly, native membrane vesicles from any type of biological membrane and liposomes that contain reconstituted protein can be attached to the SSM. Therefore, noneukaryotic membrane proteins, such as bacterial or plant membrane transporters, and intracellular membrane proteins are also suitable for this technique.

SSM-based electrophysiology has been used successfully in several studies (Bamberg et al., 1993; Seifert et al., 1993; Pintschovius and Fendler, 1999; Fendler et al., 2004; Geibel et al., 2006; Kelety et al., 2006; Bazzone et al., 2013; Garcia-Celma et al., 2013), for example to identify inhibitors of SERCA (Sadafi et al., 2014). Despite the obvious advantages and the high scientific potential of the SSM technology, this method is not yet widely used. One reason could be that suitable technical equipment was not commercially available; thus, complex instrumentation had to be manufactured by engineering workshops to use the method. Here, we worked with a commercially available complete instrument based on SSM technology (SURFE^{2}R N1; Nanion Technologies), which allows a wider community to implement the method. To demonstrate the validity and illustrate possible applications of the SSM-based method, we used the prokaryotic NCX from the archaebacterium *Methanococcus jannaschii* (NCX_Mj) as a model system. This model system is valuable because both functional data and the crystal structure of this protein are available, and the combination of both viewpoints provided insights into the structure–function relation of NCX (Liao et al., 2012). However, the functional characterization of NCX_Mj has been limited to a few qualitative flux assays using radiolabeled Ca^{2+} and liposomes containing reconstituted NCX_Mj.

The family of NCXs plays an essential role in the homeostasis of cytosolic Ca^{2+} in many different organisms. These proteins transport Ca^{2+} across the cell membrane in exchange for Na^+ with a predominant stoichiometry of 1 Ca^{2+} for 3 Na^+ (Bers, 2002). This mode of action generates the transfer of a net positive charge and thus gives rise to electrogenic transport. Other transport ratios, such as 1:1, 1:2, and 1:4 (Ca/Na) have been reported, depending on the cell type, isoform, and ionic conditions (Blaustein and Lederer, 1999). At the negative resting potential of most cell types, NCXs export Ca^{2+} across the cell membrane in exchange for Na^+ (Ca^{2+} efflux mode). In addition, NCX can operate in the reverse direction, moving Ca^{2+} into the cell (Ca^{2+} influx mode). The direction of transport depends on the driving force, which is given by the difference between the membrane potential and the reversal potential of NCX. When the membrane potential is higher than the reversal potential of the transporter, Ca^{2+} will move into the cell. For example, this situation occurs during the peak of an action potential or during ischemia if the Na^+ concentration in the cell reaches a very high level. Thus, NCX proteins contribute to the removal of excessive intracellular Ca^{2+} and the initiation, maintenance, and termination of Ca^{2+} transients (Blaustein and Lederer, 1999; Philipson and Nicoll, 2000; Sharma and O'Hal-

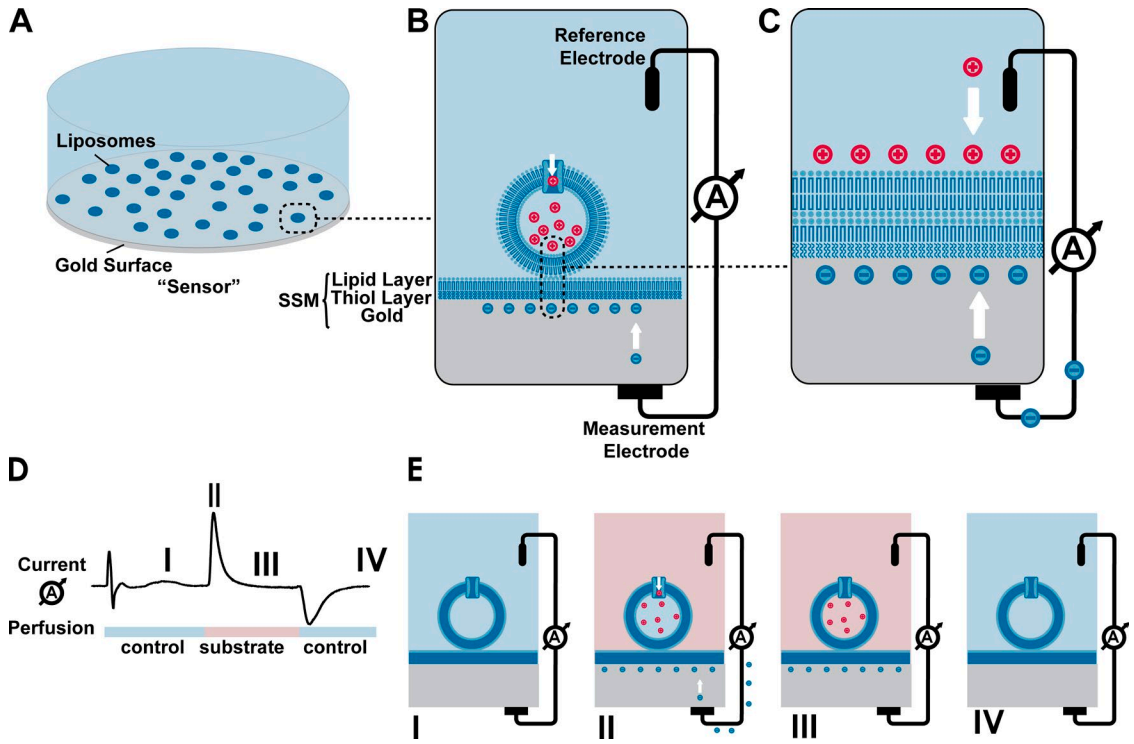

Figure 1. **Schematic illustration of SSM-based electrophysiology.** (A) Composition of an SSM-based sensor for electrophysiological recordings. A gold-coated glass plate in a small well carries an SSM. Liposomes are immobilized on the surface of the SSM. (B) Detailed view of one individual liposome on the SSM. The SSM consists of a hybrid bilayer that is formed by an alkanethiol monolayer and a phospholipid monolayer. The sulfhydryl group of the alkanethiol is covalently bound to the gold-coated surface of a glass plate supporting the SSM. Liposomes adhere to the SSM via lipid–lipid interaction. Although the cartoon depicts a multilayer structure at the liposome–SSM juncture, the exact arrangement of lipids at the contact point with the SSM is not currently known. Ions or charged substrates accumulate in the liposome as the result of the action of a transport protein. (C) Detailed view of the membrane interface. The charge accumulated inside the liposomes cannot flow through the insulating SSM but generates a measurable electron current on the gold electrode until the charge in the liposomes is electrically compensated. This mechanism is equivalent to the function of an electrical capacitor. The current flow on the gold surface is measured against a reference electrode with a constant ground potential. (D) Typical current signal recorded with SSM-based electrophysiology. The individual segments of the signal are explained in E. I: The sensor is perfused with a control buffer, which contains no substrate. II: Upon application of a suitable transportable substrate, charge accumulates inside the liposomes, thereby generating an electron current on the gold surface. III: An electrochemical equilibrium is obtained. IV: After thorough rinsing of the sensor, the activation can be repeated.

loran, 2014). NCXs are present in many organisms. In humans, these proteins are highly expressed in muscle and neuronal tissue (Khananshvili, 2013), where they are essential for many Ca^{2+}-dependent cell signaling processes, such as neurotransmission, skeletal and smooth muscle contraction, cardiac contractility (Ottolia et al., 2013), and apoptosis (Sharma and O'Halloran, 2014). Dysfunction of NCX has been associated with cardiac arrhythmia (Khananshvili, 2013) and cerebral ischemia (Pignataro et al., 2004).

Using SSM-based electrophysiology, we performed a detailed functional characterization of the prokaryotic NCX_Mj, extending the published structural data with information about the functional properties of this transporter. To increase the accessibility of this powerful technique, we provided a detailed description of our experiments and also included an in-depth Materials and methods section and an extensive troubleshooting paragraph in the supplemental text.

MATERIALS AND METHODS

Preparation of giant unilamellar vesicles (GUVs)

GUVs were prepared by electroformation (Angelova, 2000) using the Vesicle Prep Pro device (Nanion Technologies) according to the supplier's standard protocol.

A lipid solution containing 10 mM 1,2-diphytanoyl-*sn*-glycero-3-phosphocholine (DPhPC; Avanti Polar Lipids, Inc.) and 1 mM cholesterol dissolved in trichloromethane was prepared. DPhPC is a commonly used lipid for bilayer experiments and the reconstitution of isolated proteins. DPhPC membranes are very stable and good electrical insulators (Hsieh et al., 1997; Mey et al., 2009). Notably, DPhPC is contained in the native membranes of archaea (Yasmann and Sukharev, 2015). The lipid solution must be stored in a glass container and is stable at −20°C for several months. It is very important that the lipid solution does not contain any water.

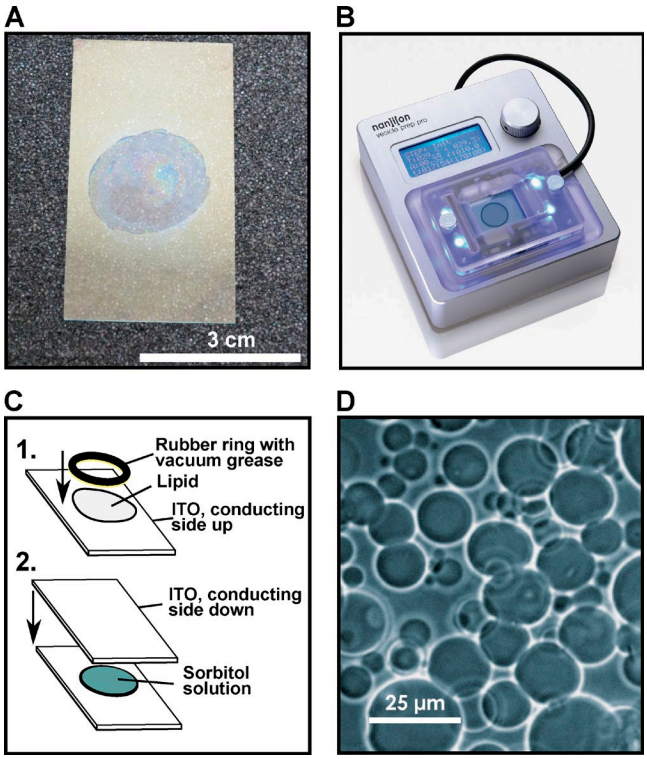

Figure 2. **Preparation of GUVs.** (A) Lipid film on the ITO glass slide after evaporation of solvent. It should form an even whitish or shimmering film. (B) Fully mounted Vesicle Prep Pro setup including the prepared slide with lipid film and sorbitol solution. (C) Cartoon of the assembling procedure of the ITO slides. In step 1, lipid is spread on the first ITO slide, and the rubber ring is mounted on top after evaporation of the solvent. In step 2, the rubber ring is filled with sorbitol solution, and the second ITO slide is layered on top. (D) GUVs obtained after the procedure.

In total, 20 µl of the lipid solution was spread on the cleaned, conducting side of an indium-tin-oxide (ITO) glass slide. After evaporation of the solvent, the lipid formed an evenly shimmering or whitish film (Fig. 2 A). The prepared slide was positioned in the Vesicle Prep Pro device. A greased rubber ring was applied around the lipid, and 270 µl of 1 M sorbitol was added slowly to the lipid layer. The second ITO slide was positioned on top of the rubber ring. The formation of air bubbles must be avoided (Fig. 2, B and C). The device was closed, and electroformation was performed using an alternating voltage of 3 V and 5 Hz for 2 h. This program is stored on the device in the default settings as "base protocol." The obtained GUVs were carefully detached from the glass surface by pipetting the sorbitol solution within the rubber ring slowly up and down after carefully removing the top glass slide. The GUV solution was diluted with 200 µl of 1 M sorbitol and stored in a plastic vial. To control the successful generation of GUVs, optical visualization with a phase contrast microscope can be performed by mixing a drop of water and a drop of GUV solution on a microscope slide (Fig. 2 D). The GUVs will burst on the glass over time. It is possible to use other methods to prepare detergent-free liposomes, but adaption of the reconstitution protocol will be required. The usage of other lipids is possible as well but also requires optimization of the protocol.

Preparation of human NCX1-containing membrane fragments

A membrane preparation of NCX1 (SLC8A1) expressed in HEK-293 cells was performed as previously described (Krause et al., 2009). In brief, cells were kept in culture under standard conditions (5% CO_2, 37°C) and disrupted mechanically. The membrane was separated from cores and mitochondria using several centrifugation steps and was purified using a sucrose gradient. Membranes were frozen at −80°C and prepared for experiments as described previously (Geibel et al., 2006).

Purification of NCX_Mj protein

Protein was purified as described in detail by Liao et al. (2012) in the supplement of the initial publication reporting the structure of NCX_Mj. In brief, NCX from *M. jannaschii* was expressed in *Escherichia coli*, and the cells were lysed mechanically. The lysate was incubated with *n*-dodecyl-β-D-maltopyranoside for protein extraction, and the protein was collected with a TALON Co^{2+} affinity column. Hexahistidine tags were removed, and the protein was further purified and concentrated by gel filtration (Superdex-200, 10/300 GL column; GE Healthcare). The peak fraction at ∼13.2 ml was collected and mainly contained the monomer of NCX_Mj. The protein was further concentrated to 1–2 mg/ml using an Amicon Ultra-4 centrifugal filter (MWCO 100 kD).

Reconstitution of NCX_Mj protein in GUVs

NCX_Mj was successfully reconstituted directly into the GUVs. For reconstitution, 10 µl of 2.5 µg/µl detergent-solubilized protein (0.6–1 mM DDM) was added to 200 µl GUV solution, vortexed for 5 s, and incubated at room temperature for 30 min. The solution was then incubated for another 2 h at 4°C. Next, 10 mg Bio-beads (Bio-Rad Laboratory) was added to the vesicles to remove detergent and incubated overnight at 4°C. The solution was then transferred to a new vial to remove the Bio-beads. Protein-containing vesicles were used immediately or stored at 4°C for a maximum of 5 d. Similar reconstitution approaches have been described previously, e.g., by Kreir et al. (2008). Control experiments to optimize the ratio of the lipid and protein concentrations during the reconstitution process were performed, and they indicated that 10 µl of 2.5 µg/µl protein solution gave the optimal results (see Fig. 6 C). This protocol was not optimized for an oriented insertion of the protein into the liposomes.

Thiol coating of the sensors blanks

The combination of SSM and immobilized liposomes or membrane fragments is referred to as the sensor. All experiments were performed using the SURFE^{2}R N1 device and the matching N1 sensor blanks (Nanion Technologies). The sensor blanks included a 3-mm-diameter gold surface inside a small well, and the gold surface was already coated with an alkanethiol layer. This layer was refreshed in advance of SSM assembly to enable the formation of a stable and electrically dense hybrid lipid layer. This was done by incubating the sensor blank with 50 µl of 0.5 mM 1-octadecanethiol dissolved in isopropanol for 30 min. Isopropanol was heated slightly to dissolve the octadecanethiol. The prepared octadecanethiol solution was stored at room temperature in the dark in a glass vial. The sensor blanks were enclosed in a small container during incubation to prevent evaporation of the solvent. After the incubation period, the sensor well was rinsed once with isopropanol and twice with water (ddH_2O), drained by tapping on a tissue, and left for 30 min at room temperature to dry.

Preparation of the SSM

For this step, 7.5 µg/µl DPhPC was dissolved in *n*-Decane. The lipid solution can be stored at −20°C or −80°C for several months in a glass vial. It is critical for the solution to remain free of water. 1.5 µl was added to the thiol-coated gold surface. The pipette should not touch the surface. The lipid formed a small drop on the pipette tip, and the drop spread out as soon as it touched the hydrophobic gold surface. Immediately, 80 µl of loading buffer was carefully added. The GUV solution was sonicated for 30 s in a water bath, and 8 µl was added directly to the SSM by submerging the pipette in the buffer. Afterward, the sensors were centrifuged for 1 h at 2,200 *g*. The sensors showed activity for several days when stored at 4°C. The quality of the SSM was ensured by selecting sensors with appropriate values of conductance σ and capacitance *C*. These values reflect the electrical properties of the hybrid lipid layer. The sensors should have a conductance <3 nS and capacitance <20 nF. Higher values indicate a perforated lipid layer or a thick lipid multilayer, which manifests itself in high noise and sensitivity to mechanical and chemical disturbances. The threshold values were evaluated empirically. The SURFE^{2}R N1 device includes default functions to perform these measurements. In brief, certain voltage protocols were applied to the SSM, and σ and *C* were calculated from the current response (Fig. 3).

Electrophysiological measurements

Prepared sensors were inserted into the Faraday cage of the SURFE^{2}R N1 device (Fig. 4, A and C), and buffers were applied via its fast automatic perfusion system (Fig. 4 D). A protocol was generated in advance that defined the buffer positions, application speed, and

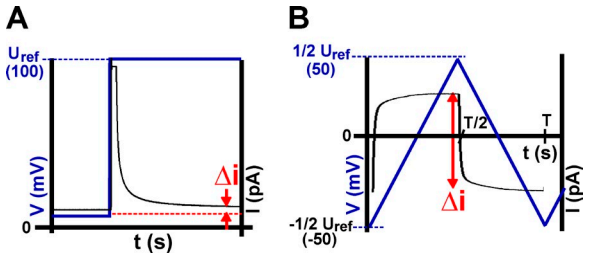

Figure 3. **Determination of the capacitance and conductance of an SSM sensor.** Voltage traces are displayed in blue; current traces are displayed in black. (A) Conductance measurement. A voltage step from 0 to 100 mV is applied, and the resulting offset current is measured. The conductance can be calculated from the offset current: $\sigma = \Delta i/U_{ref}$. (B) Capacitance is determined by the application of a periodic and symmetric triangular voltage command (symmetric up and down sloping voltage ramp) and the recording of the resulting current response. A typical current trace is depicted above. From the current amplitude, the capacitance can be calculated as $C = \Delta iT/4U_{ref}$, where T stands for the period of the delta voltage.

times. The perfusion system of the SURFE^{2}R N1 allows the application and exchange of buffers in a continuous liquid flow. The following buffer addition sequence was used for all experiments. First, control buffer was applied for 2 s with a flow rate of 200 µl/s. This step was performed to wash away the loading buffer in the sensor well and to generate a clean baseline before NCX_Mj activation. With the same flow rate of 200 µl/s, the activation buffer was then applied for 2 s and washed out again by control buffer (2 s). During those 6 s, the current response was recorded. After the recording, the sensor was rinsed with loading buffer. The protocol described can be adapted to any SSM-based electrophysiological system.

Buffer solutions

Buffers were prepared according to Table 1. EGTA was added to all buffers to set the free Ca^{2+} concentration in Ca^{2+}-containing buffers or to chelate the trace amount of free Ca^{2+} in Ca^{2+}-free buffers. The free Ca^{2+} concentration was calculated with MaxChelator (Chris Patton, Stanford University), a widely used software tool for determining the free metal concentrations in the presence of chelators (Bers et al., 2010). JavaScript web version 1.2 using constants from National Institute of Standards and Technology (NIST) Database 46 version 8 was used. For Ca^{2+} affinity experiments, Mg^{2+} was removed from the solutions. For divalent inhibition experiments, EGTA was removed. For selectivity experiments, Ca^{2+} and Na^+ were substituted by the ions of interest. Variations of the buffer properties can cause physical disturbances of the large and sensitive electrode, which can resemble signals. Therefore, it is important to minimize differences in the individual buffers with regards to pH, osmolarity, and ionic

Table 1. **Buffer composition**

Outward $I_{Na/Ca}$			Inward $I_{Na/Ca}$		
Loading buffer	**Control buffer**	**Activation buffer**	**Loading buffer**	**Control buffer**	**Activation buffer**
30 mM HEPES	30 mM HEPES	30 mM HEPES	30 mM HEPES	30 mM HEPES	30 mM HEPES
1 mM EGTA	1 mM EGTA	1 mM EGTA	1 mM EGTA	1 mM EGTA	1 mM EGTA
4 mM $MgCl_2$	4 mM $MgCl_2$	4 mM $MgCl_2$	4 mM $MgCl_2$	4 mM $MgCl_2$	4 mM $MgCl_2$
140 mM NaCl	280 mM sorbitol	280 mM sorbitol	220 mM sorbitol	180 mM sorbitol	180 mM sorbitol
pH 7.4 (NMDG)	pH 7.4 (NMDG)	100 µM $CaCl_2$ (free)	20 mM $CaCl_2$	60 mM choline Cl	50 mM choline Cl
		pH 7.4 (NMDG)	pH 7.4 (NMDG)	pH 7.4 (NMDG)	10 mM NaCl
					pH 7.4 (NMDG)

strength. For this purpose, 10 mM choline chloride was added to the control buffer (inward $I_{Na/Ca}$) to compensate for the sodium-induced difference in osmolarity. The signal baseline was further stabilized by the addition of 50 mM choline chloride to both the control and activation buffers.

Data analysis

The net movement of cations out of the vesicles into the sensor lumen is displayed as a positive current, which matches the patch-clamp convention of reporting an outward cation flux as a current with positive sign. Raw data were exported as ASCII files, and analysis was performed using the scientific graphing and data analysis program IGOR Pro 6 (WaveMetrics). Peak currents were determined using a peak detection algorithm. For every mean value, only results from different sensors were compared. The errors indicate the SEM. Concentration response relationships for inhibition and apparent affinity were obtained by perfusion of the sensors with increasing ion concentrations. Data were normalized to the maximum amplitude and described by fitting to a Hill function (Boyman et al., 2009; Ottolia et al., 2009):

$$I(c) = \frac{1}{1 + \left(\frac{c}{K_d}\right)^{nH}}.$$

The reported IC_{50} and apparent K_d values and the corresponding errors were calculated by fitting each test series to a Hill function and subsequently averaging the individual values. The number of experiments performed on independent sensors is indicated as *n*.

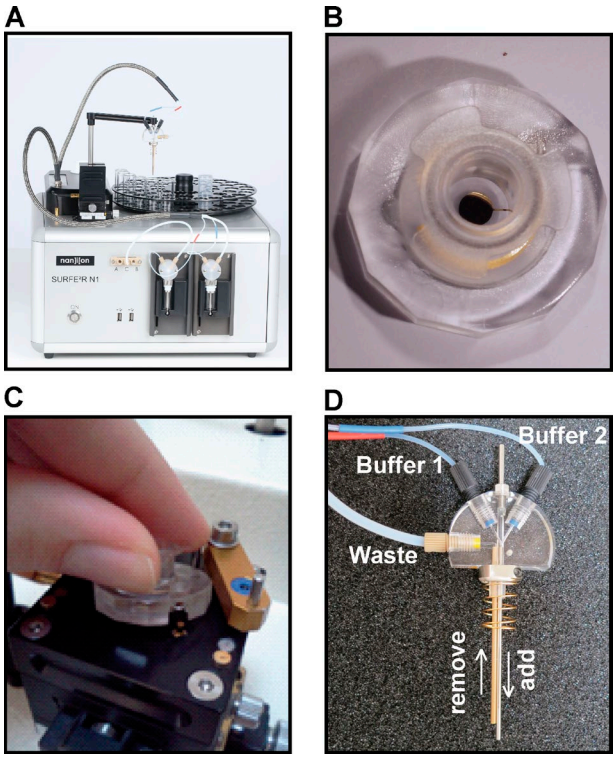

Figure 4. **SURFE²R N1 device.** (A) The complete device (screen with the user interface not shown). (B) Sensor blank with gold surface included in the well. (C) Mounting the sensor onto the Faraday chamber of the device. (D) The perfusion system of the device. Two separate pipettes add and remove liquid simultaneously. The Y-shaped feeding channels enable the application of two different buffers in a continuous flow.

Online supplemental material

In the supplemental material, further details of the SSM-based electrophysiology technique are provided for researchers who wish to establish the method in their own laboratory. The first section includes a detailed troubleshooting section, which is subdivided into the topics GUV formation, reconstitution, SSM preparation, and measurement. Table S1 shows preparation of GUVs. Table S2 shows reconstitution of NCX_Mj protein in GUVs. Table S3 shows sensor thiolization. Table S4 shows SSM preparation. Table S5 shows electrophysiological ion current measurement. The second section contains general instructions about how to design suitable buffer solutions when setting up a new SSM-based assay from scratch. Table S6 shows substrate and ion substitutes. Online supplemental material is available at http://www.jgp.org/cgi/content/full/jgp.201611587/DC1.

RESULTS

To characterize NCX_Mj using SSM-based electrophysiology, the protein was purified from *E. coli* and reconstituted into unilamellar liposomes. An SSM was generated by first coating a 3-mm gold electrode with

octadecanethiol and subsequently with a phospholipid monolayer. The sensor was finalized by immobilization of protein-containing liposomes on the SSM. NCX-containing sensors were inserted into the measuring chamber and perfusion system of the SURFE^{2}R N1, which allows rapid application and exchange of extra-liposomal buffers in a continuous flow.

Lipid vesicles were loaded with 140 mM Na^+ during the preparation of the SSM sensor. At the beginning of the electrophysiological experiment, stable baseline conditions were established by the application of a Na^+- and Ca^{2+}-free control buffer via the perfusion system (Fig. 5 A, step 1). This step ensured clearly defined starting conditions, established a strong Na^+ gradient, and clearly separated the signal of interest from possible mechanical disturbances, which could be caused by the onset of the perfusion. $I_{Na/Ca}$ was subsequently activated by application of Ca^{2+}-containing buffer (100 µM free Ca^{2+}, Na^+ free; Fig. 5 A, step 2). The application of external Ca^{2+} to vesicles containing Na^+ generated a transient outward exchanger current $I_{Na/Ca}$. Finally, the Ca^{2+}-containing buffer was washed out with a Ca^{2+}-free control buffer (Fig. 5 A, step 3). This activation cycle was highly reproducible, e.g., it could typically be repeated at least 10 times. The outwardly directed $I_{Na/Ca}$ indicates that NCX_Mj generates a net cation flux out of the liposomes. This finding is consistent with a net flux of Na^+ out of the vesicles, most likely caused by the dominant stoichiometry of 3 Na^+ ions to 1 Ca^{2+} ion that is well known for other members of the NCX family (Bers, 2002). The specific buffer composition can be found in Materials and methods (Buffer solutions).

The aforementioned procedure allows the application of different Ca^{2+} concentrations, various other divalent ions, and inhibitors. However, it does not allow straightforward alteration of the Na^+ concentration because Na^+ ions are present on the luminal side of the vesicles. To investigate the apparent Na^+ affinity, $I_{Na/Ca}$ was induced as a net inward cation flux (Fig. 5 B). To achieve this current, the ion concentrations on both sides of the membrane were inverted. The sensors were prepared in a Na^+-free loading buffer containing 20 mM Ca^{2+}. NCX_Mj was activated by rapid application of Na^+-containing buffer (10 mM). The external application of Na^+ to Ca^{2+}-containing vesicles then generated a transient inward $I_{Na/Ca}$, which was produced by the electrogenic transport of Na^+ in and Ca^{2+} out of the vesicles.

To statistically validate the reproducibility and efficiency of the method, including the success of reconstitution and the success of sensor preparation, different batches of NCX_Mj-containing liposomes were prepared, and the $I_{Na/Ca}$ amplitudes were compared. Themean Ca^{2+}-induced outward $I_{Na/Ca}$ amplitude was 830 ± 101 pA (n = 10 batches), and the Na^+-induced inward $I_{Na/Ca}$ amplitude was −1,116 ± 125 pA (n = 12 batches). In contrast, when protein-free liposomes were

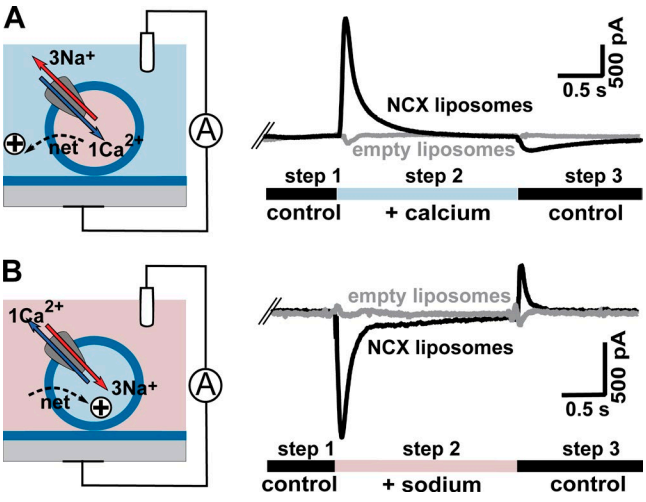

Figure 5. **SSM-based NCX_Mj assays in liposomes.** A cartoon view of the SSM setup is depicted on the left; the resulting current is depicted on the right. The accurate composition of all buffers can be found in Materials and methods (Buffer solutions). (A) NCX_Mj is reconstituted into lipid vesicles containing Na^+. A transient outward cation net flux $I_{Na/Ca}$ is activated by the application of a buffer containing Ca^{2+}. (B) Same as in A, but in this panel, the vesicles contain Ca^{2+}, and the transport is activated by the application of external Na^+. The signal is inverted as the result of an opposite Na^+ flux.

used for the control experiments, the mean peak current amplitudes were −72 ± 6 pA (Ca^{2+}-containing vesicles) and −83 ± 21 pA (Na^+-containing vesicles). These results indicate a ratio of signal to nonspecific baseline artifacts of ∼1:10 (Fig. 6 A). The quality of each prepared sensor was controlled by determining the capacitance and conductance of the SSM; these parameters reflect the condition of the lipid layer. Sensors with a capacitance >20 nF or conductance >3 nS were discarded. The mean capacitance and conductance of the sensors used for experiments were 13.9 ± 1 nF and 1.2 ± 0.1 nS, respectively (Fig. 6 B). Less than 10% of all prepared sensors failed this quality control. To optimize the protein reconstitution process, the protein concentration during reconstitution was varied. These experiments revealed that the NCX_Mj signal increases in parallel with the protein concentration and saturates at 125 ng/µl (Fig. 6 C). Although we observed a strong dependence of NCX_Mj activity on the input protein concentration used for the experiment, there is no straightforward way to actually quantify the fraction of active protein successfully reconstituted in the membrane of the vesicles and the number of liposomes per sensor. Given that all liposomes adhere to the sensor and assuming a turnover rate of 5,000/s (determined for eukaryotic NCX1 [Hilgemann, 1996]), we can estimate a reconstitution rate of 0.2×10^{-2}%. There are several possible explanations for this observed low reconstitution rate. Likely, the reconstitution rate could be underestimated, either because of the insertion of

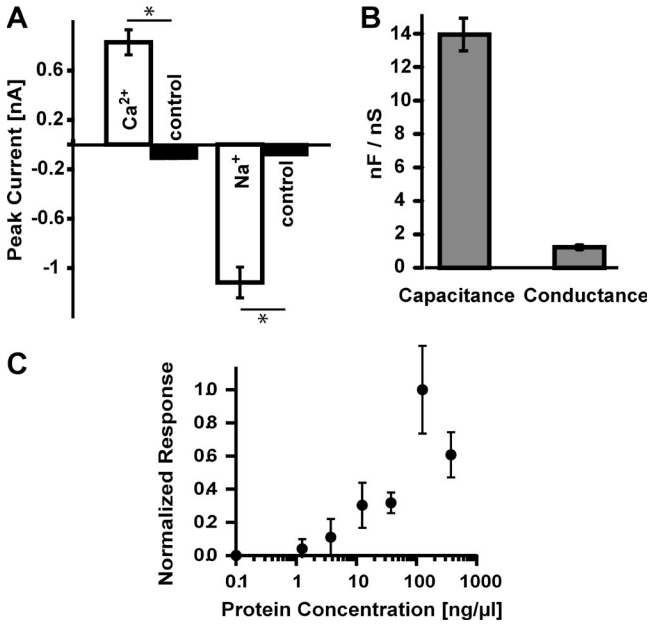

Figure 6. **Control experiments to evaluate the reconstitution success and SSM quality.** (A) Mean peak $I_{Na/Ca}$ amplitude of different liposome batches (n = 10). *, P < 0.001. (B) SSM properties. The mean capacitance was 13.9 ± 1 nF, and the mean conductance was 1.2 ± 0.1 nS (n = 17). (C) Optimization of the protein reconstitution process by testing different protein to lipid ratios. The detergent concentration was adjusted to 50 µM. The lipid concentration was 0.375 mg/ml throughout the experiment. The most effective concentration was 125 ng/µl protein (n = 3). Errors indicate the SEM.

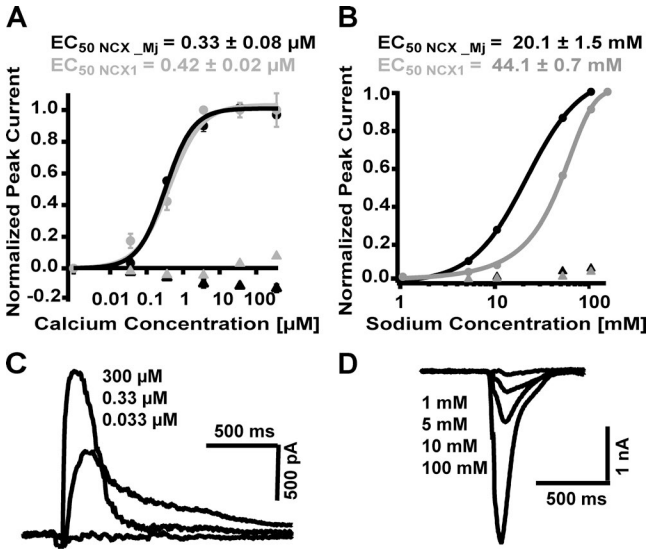

Figure 7. **Apparent Ca^{2+} and Na^+ affinities of NCX_Mj and human NCX1.** EC_{50} was calculated separately for each sensor and subsequently averaged. Control experiments (triangles) were performed with empty liposomes/parental HEK cell membranes. The current response of the control measurements was averaged and normalized to the mean current response of NCX using 100 µM Ca^{2+}/100 mM Na^+. (A) The apparent Ca^{2+} affinity was measured using vesicles loaded with 140 mM Na^+. An outward $I_{Na/Ca}$ was activated by the application of solution containing differing free Ca^{2+} concentrations as indicated. EC_{50NCX_Mj} = 0.33 ± 0.08 µM and EC_{50NCX1} = 0.42 ± 0.02 µM (n = 5). Hill coefficients: 1.1 ± 0.18 for NCX_Mj and 1.06 ± 0.13 for NCX1. (B) Apparent Na^+ affinity was determined using vesicles loaded with 20 mM Ca^{2+}. An inward $I_{Na/Ca}$ was activated by the application of increasing Na^+ concentrations as indicated. EC_{50NCX_Mj} = 20.1 ± 1.5 mM and EC_{50NCX1} = 44.1 ± 0.7 mM (n = 4). Hill coefficients: 1.7 ± 0.07 for NCX_Mj and 1.4 ± 0.04 for NCX1. (C) Representative current traces of NCX_Mj $I_{Na/Ca}$ evoked by different Ca^{2+} concentrations. (D) Representative current traces induced by Na^+. Errors indicate the SEM.

nonfunctional protein or the precipitation of a major fraction of the protein during the reconstitution process; the precipitated protein would not be integrated into the vesicle. Otherwise, the reconstitution capacity, the stability, and the process of protein insertion of the specific liposome type used likely differs from other liposome types, mainly because of the large size and the complete absence of detergent. However, if we assume a 100% reconstitution rate and 100% adhesion efficiency of the added liposomes to the sensor, we can estimate a minimum turnover rate of $\sim 1.03 \times 10^{-3}$/s.

We used the established NCX_Mj activation modes of inward and outward $I_{Na/Ca}$ (Fig. 5) to determine apparent Ca^{2+} and Na^+ affinity of NCX_Mj (Fig. 7). For the determination of the apparent Ca^{2+} affinity, the liposomes were loaded with 140 mM Na^+ (outward $I_{Na/Ca}$) while varying extra-liposomal Ca^{2+} concentrations were applied. For the determination of the apparent Na^+ affinity, the liposomes were loaded with 10 mM Ca^{2+} (outward $I_{Na/Ca}$) while varying extra-liposomal Na^+ concentration. In a subset of analogous experiments, the results were compared with human NCX1, which is present in membrane fragments from HEK cells expressing NCX1. Control experiments were performed with empty liposomes for NCX_Mj or with membrane fragments generated from the parental cell line for NCX1. The recording solutions were identical in all these subsets of experiments. These experiments revealed a half-activating Ca^{2+} concentration of 0.33 ± 0.08 µM (n = 5) for NCX_Mj and of 0.42 ± 0.02 µM (n = 3) for human NCX1. The half-activating Na^+ concentrations were 20.1 ± 1.5 mM (n = 4) for NCX_Mj and 44.1 ± 0.7 mM (n = 3) for NCX1 (Fig. 7). The identified apparent affinities should be considered a weighted mean of both transport modes, reflecting the nonoriented integration of the purified protein into the liposomes.

It is well known that NCXs are inhibited by divalent ions (Iwamoto and Shigekawa, 1998; Blaustein and Lederer, 1999). To investigate this characteristic of NCX_Mj using our method, we analyzed the effects of Cd^{2+}, Mn^{2+}, and Mg^{2+} on $I_{Na/Ca}$. This was achieved by the addition of the respective divalent ion to all buffers. The experiments revealed that the $I_{Na/Ca}$ activated by either Ca^{2+} or Na^+ was fully blocked by 100 µM Cd^{2+} (Fig. 8 A). The IC_{50} of the Cd^{2+}-dependent inhibition of $I_{Na/Ca}$ was 2.2 ± 0.3 µM (n = 3; Fig. 8 B). The Cd^{2+} inhibi-

tion was partially reversible, with a 60% recovery of the $I_{Na/Ca}$ amplitude relative to the control (Fig. 8 C). Mn^{2+} caused only a partial inhibition of $I_{Na/Ca}$, showing an approximate 10% decrease in the presence of 100 µM Mn^{2+} compared with the control. Mg^{2+} induced no significant inhibition at concentrations of 100 µM and <10% inhibition at 4 mM. Because the physiologically most relevant divalent cations in the cell are Ca^{2+} and Mg^{2+}, we further analyzed the apparent Ca^{2+} affinity in both the absence and presence of 100 µM and 4 mM Mg^{2+}. In the presence of 4 mM Mg^{2+}, the Ca^{2+}-dependent activation of $I_{Na/Ca}$ was sigmoidal and shifted in parallel toward higher Ca^{2+} concentrations (Fig. 8 D). This finding could indicate a specific interaction of the Mg^{2+}- with the Ca^{2+}-binding site or with the transport mechanism. It is also possible that a change in surface potential could contribute to or completely account for the observed shift.

Furthermore, we used the SSM-based method to investigate the selectivity of NCX_Mj for some monovalent cations of main group 1 (alkaline metals) and some divalent cations of main group 2 (alkaline earth metals). Mg^{2+}, Sr^{2+}, and Ba^{2+} were tested as Ca^{2+} substitutes; K^+, Rb^+, and Li^+ were tested as Na^+ substitutes. As a positive control, experiments using Na^+ and Ca^{2+} were performed simultaneously. The $I_{Na/Ca}$ amplitude of the tested cations was normalized to either the Na^+ (monovalent cations)- or the Ca^{2+} (divalent cations)-induced amplitude for comparability. Negative control experiments were performed using protein-free liposomes. By preloading the liposomes with high concentrations of the respective cations (140 mM for monovalent cations, 20 mM for divalent), we first tested whether these cations could serve as alternative substrates at very high concentrations (Fig. 9, A and B). This procedure was selected to avoid large differences in the ionic concentrations of the control and substrate-containing buffers, which could cause a physical disturbance of the current baseline (for detailed information, see supplement text section Buffer composition instructions for new assays). In liposomes loaded with 20 mM of the respective divalent ions, application of buffer containing 10 mM Na^+ induced an inward $I_{Na/Ca}$ in all cases with an amplitude significantly higher than that of the negative control measurements of protein-free liposomes (Fig. 9 A). Liposomes loaded with Sr^{2+} generated an even higher $I_{Na/Ca}$ amplitude than did Ca^{2+}-loaded liposomes (145 ± 15%). The Mg^{2+}- and Ba^{2+}-mediated inward $I_{Na/Ca}$ amplitudes were slightly lower than the Ca^{2+} current amplitudes (63 ± 3% and 78 ± 3%). These results indicate a low selectivity of the transporter for Ca^{2+}. Analogous experiments were performed for monovalent cations (Fig. 9 B). Vesicles were loaded with 140 mM of the respective monovalent cations, and an outward $I_{Na/Ca}$ was induced by the application of extra-liposomal solution containing 100 µM Ca^{2+}. Remarkably, in addition to Na^+, only Li^+-loaded liposomes gave rise to an outward $I_{Na/Ca}$ (23 ± 5%) significantly higher than that of protein-free control liposomes, whereas Rb^+ and K^+ did not, indicating a high selectivity of the transporter for Na^+.

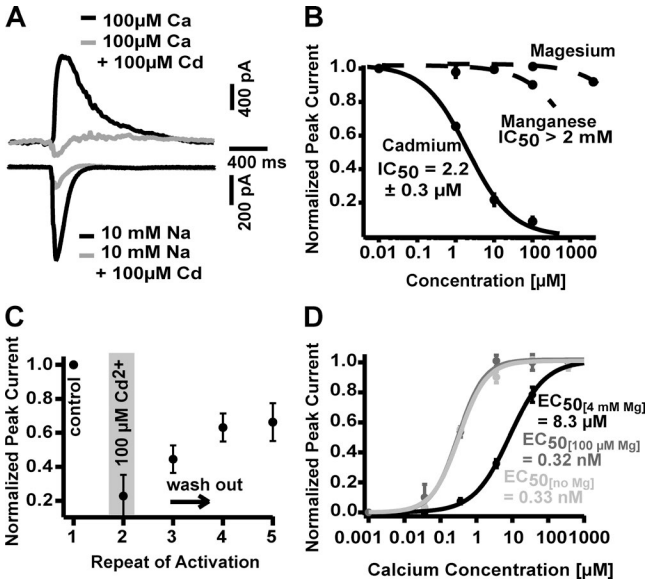

Figure 8. **Inhibition of NCX_Mj by divalent cations.** (A) Representative traces of Na^+- and Ca^{2+}-activated NCX_Mj currents. Both are inhibited by 100 µM Cd^{2+}. (B) Concentration response curves of Cd^{2+}, Mg^{2+}, and Mn^{2+} in the presence of 100 µM Ca^{2+}. Cd^{2+} caused a strong inhibition at low concentrations (IC_{50} = 2.2 ± 0.3 µM, Hill = 0.8 ± 0.05, n = 3), whereas Mn^{2+} decreased $I_{Na/Ca}$ by only 10% at 100 µM (n = 2). Mg^{2+} inhibited $I_{Na/Ca}$ by <10% at a concentration of 4 mM. (C) Reversibility of Cd^{2+} inhibition. After activation of $I_{Na/Ca}$ by Ca^{2+} and subsequent block by Cd^{2+} (100 µM, duration: 2 s), only partial recovery of $I_{Na/Ca}$ upon washout of Cd^{2+} was observed. (D) Apparent Ca^{2+} affinity of NCX in the absence and presence of 100 µM or 4 mM Mg^{2+}. The Ca^{2+} affinity of NCX_Mj did not change in the presence of 100 µM Mg^{2+}. In the presence of 4 mM Mg^{2+}, the Ca^{2+}-induced NCX_Mj activity was shifted toward higher Ca^{2+} concentrations. Hill coefficients: 0.9 ± 0.02 (4 mM), 1.2 ± 0.13 (100 µM), and 1.1 ± 0.18 (no Mg^{2+}). Errors indicate the SEM.

In a second set of experiments, the cations of interest were applied to the extra-liposomal side of the vesicles in physiologically relevant concentrations. First, liposomes were loaded with 140 mM Na^+, and extra-liposomal buffer containing 100 µM of the respective divalent cation was applied (Fig. 9 C). Among the divalent cations tested, only Ca^{2+} and Sr^{2+} induced an outward $I_{Na/Ca}$, whereas Mg^{2+} and Ba^{2+} did not. Surprisingly, the Sr^{2+}-induced outward $I_{Na/Ca}$ amplitudes were higher than the Ca^{2+}-induced current amplitudes (168 ± 51%, P = 0.039). Furthermore, liposomes were loaded with 20 mM Ca^{2+}, and extra-liposomal buffer containing 10 mM monovalent cations was applied (Fig. 9 D). No monovalent cation was able to substitute Na^+ at a concentration of 10 mM. Li^+ generated a small NCX-like inward $I_{Na/Ca}$. In an additional subset of experiments, the Cd^{2+} sensitivity of the currents induced by Ca^{2+} and

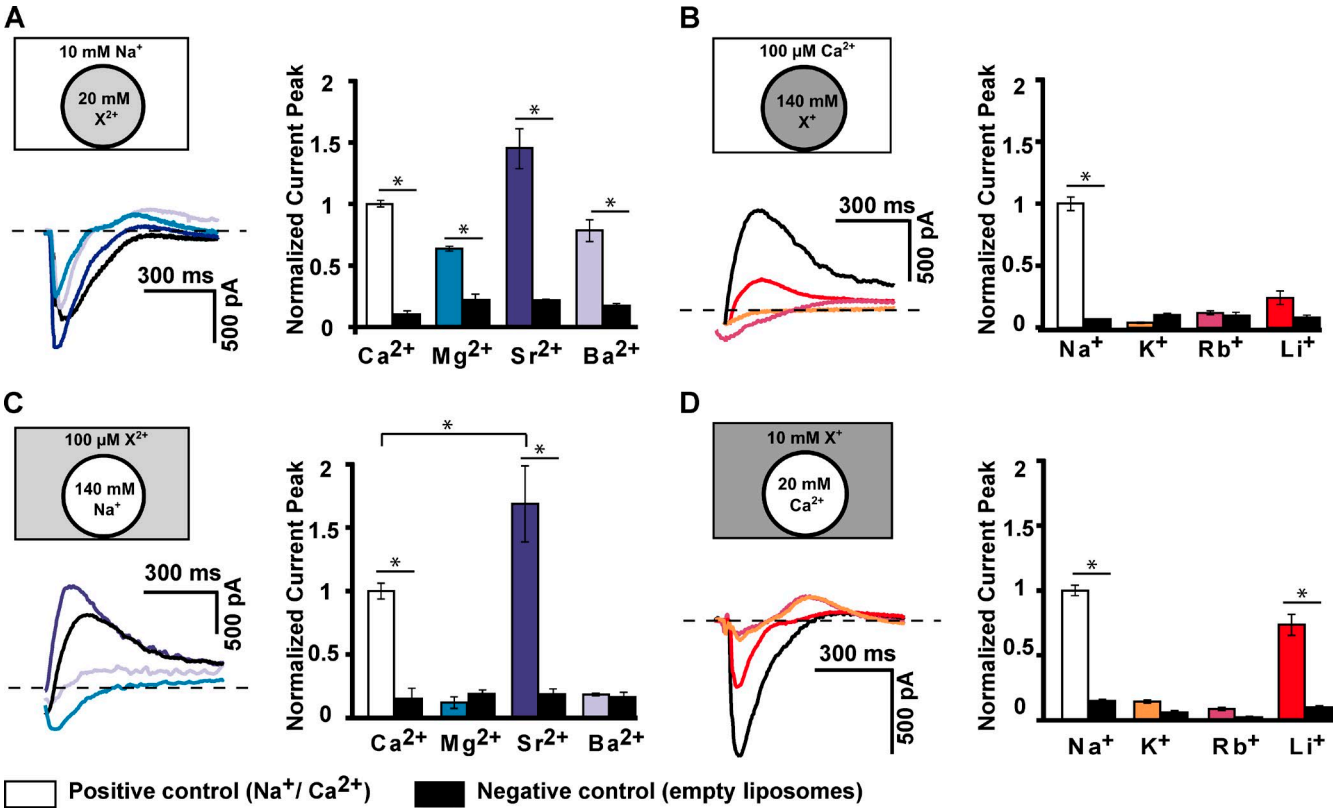

Figure 9. **Ca^{2+} and Na^+ selectivities of NCX_Mj.** Negative control experiments are represented by black columns. *, $P < 0.05$. (A) NCX_Mj-containing liposomes were loaded with 20 mM of different divalent cations (Ca^{2+}/Mg^{2+}/Sr^{2+}/Ba^{2+}), and the activation of an inward $I_{Na/Ca}$ was induced by the application of extra-liposomal buffer containing 10 mM Na^+. (B) Liposomes were loaded with 140 mM of different monovalent cations (Na^+/K^+/Rb^+/Li^+), and the activation of an outward $I_{Na/Ca}$ was induced by the application of extra-liposomal buffer containing 100 µM Ca^{2+}. (C) Liposomes were loaded with 140 mM Na^+, and an outward $I_{Na/Ca}$ was activated by the application of a solution containing 100 µM of the respective divalent cation. The application of Mg^{2+} generates a small negative peak resulting from nonspecific interference with the gold electrode; control liposomes showed the same behavior. (D) Vesicles were loaded with 20 mM Ca^{2+}, and an inward $I_{Na/Ca}$ was activated by the application of solution containing 10 mM of the monovalent cation. Errors indicate the SEM. n = 3–5 for every experiment.

Na^+ substitutes was tested. The Sr^{2+}-, Mg^{2+}-, Ba^{2+}-, and Li^+-generated outward and inward currents in the presence and absence of 100 µM Cd^{2+} were compared. Just as observed for the Ca^{2+}-induced $I_{Na/Ca}$, the inward and outward currents carried by Sr^{2+}, Mg^{2+}, and Ba^{2+} were inhibited by Cd^{2+}, whereas the Li^+-generated currents were insensitive to Cd^{2+}. Collectively, these results indicate that NCX transporters are highly selective for Na^+, whereas the selectivity for Ca^{2+} is substantially lower.

Because replacement of Ca^{2+} by Sr^{2+} resulted in a prominent $I_{Na/Ca}$, we determined the apparent Sr^{2+} affinity (Fig. 10). We found that the half-activating concentration of Sr^{2+} was 19.5 ± 4.0 µM (n = 3). In conclusion, Sr^{2+} generated higher current amplitudes than Ca^{2+}; however, the apparent affinity of NCX_Mj for Sr^{2+} was lower than for Ca^{2+} (0.33 µM).

DISCUSSION

In this study, we used the archaeal sodium–calcium transporter protein NCX_Mj as a model system to demonstrate the successful implementation of an SSM-based electrophysiological approach. By applying this method, we obtained an accessible, robust, and flexible assay that is suitable for the electrophysiological characterization of the prokaryotic transporter protein.

The SSM-based technology is characterized by a high overall success rate of >90%, as indicated by a suitable conductance and capacity (<3 nS, <20 pF) of the prepared SSM sensors and the ability to generate reproducible NCX_Mj transport currents with a satisfactory signal to noise ratio (>10:1). Currents up to 2 nA amplitude were measured. The transporter current could be activated repetitively with a stable amplitude at least 10 times per sensor, enabling complete EC_{50} or IC_{50} determination using the same population of proteins.

Our approach allowed us to obtain a detailed electrophysiological characterization and comparison of different NCX isoforms. We found that NCX_Mj-dependent transport is electrogenic, consistent with the proposed main transport stoichiometry of 3 Na^+ to 1 Ca^{2+} (Liao et al., 2012). The apparent affinities for

Na^+ and Ca^{2+} are in the expected range for a member of the NCX family (Blaustein and Lederer, 1999). NCX_Mj is inhibited by divalent cations; Cd^{2+} displayed the highest blocking effect, with an IC_{50} value of 2.2 ± 0.3 µM (n = 3). This value is somewhat lower than the published values of 30–60 µM for eukaryotic NCX1–3, which were determined by Ca^{2+} uptake assays (Iwamoto and Shigekawa, 1998) and considerably lower than the IC_{50} of ~0.4 mM determined for NCX_Mj by Liao et al. (2012) (Ca^{2+} uptake assay). A possible reason for the considerably lower values observed by the SSM method than by the radioisotope labeled flux assay is differences in the experimental conditions, particularly the time scale and read-out method of the two approaches. The exact reason is not known. In addition, we observed a blocking effect of Mn^{2+} and Mg^{2+} at high concentrations, which is in agreement with experiments performed on eukaryotic NCX isoforms (Iwamoto and Shigekawa, 1998; Blaustein and Lederer, 1999). In another set of experiments, we investigated the selectivity for Na^+ and Ca^{2+}. NCX_Mj showed a high selectivity for Na^+ compared with other monovalent alkali cations, whereas Sr^{2+} substituted for Ca^{2+} very effectively at low concentrations. Although the apparent Sr^{2+} affinity was lower than the apparent Ca^{2+} affinity, the observed current amplitudes generated by Sr^{2+} were significantly higher. Mg^{2+} and Ba^{2+} were able to substitute for Ca^{2+} at high concentrations; this finding is compatible with the described properties of eukaryotic NCXs (Blaustein and Lederer, 1999).

In direct comparison of NCX1 and NCX_Mj, the apparent Ca^{2+} and Na^+ affinities were almost identical. Together with the observed typical NCX characteristics, this result suggests a very close functional similarity of the archaeal isoform NCX_Mj to the well-described eukaryotic NCX isoforms. This finding is particularly noteworthy because prokaryotic NCX isoforms lack the f-loop, a large intracellular regulatory domain. Therefore, these findings not only refine our knowledge of the electrophysiological properties of the archaeal NCX isoform, but also confirm that the NCX_Mj crystal structure (Liao et al., 2012) is a valid model for other NCX isoforms.

Our results primarily demonstrate that SSM-based electrophysiology is well suited for the detailed functional characterization of transport proteins, as exemplified by NCX_Mj. The method enabled straightforward real-time measurements of the transport currents, which were characterized by high stability and flexibility (regarding buffer composition, transported substrates, and source of transport protein). These features qualify the SSM-based approach as a valuable alternative to conventional patch-clamp experiments, particularly for prokaryotic or intracellular transporters or for proteins that generate currents below the resolvable amplitude. In particular, we believe that SSM-based electrophysiology provides a convenient approach that complements structural studies, allowing functional experiments with the same protein sample. Furthermore, in our opinion, the method has, because of its robustness and scalability, great potential as a tool for drug discovery. We hope that the SSM-based approach will be adapted for studies of other electrogenic transporters, and we are convinced that the interesting features of the method will stimulate its propagation in the future.

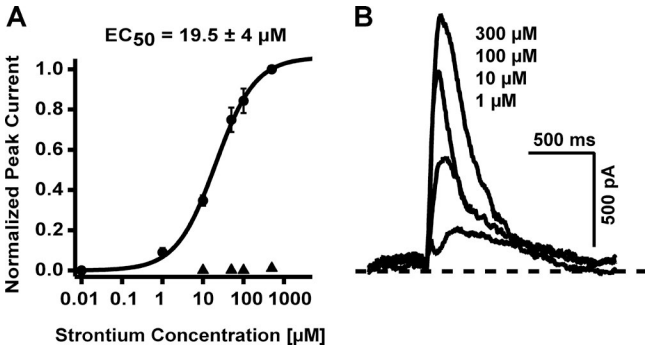

Figure 10. **Apparent Sr^{2+} affinity of NCX_Mj.** (A) Application of different Sr^{2+} concentrations to Na^+-loaded liposomes (140 mM Na^+). EC_{50} was calculated to be 19.5 ± 4 µM. Hill coefficient: 0.9 ± 0.07 (n = 3). Control experiments in protein-free liposomes are depicted as triangles. (B) Representative current traces of the outward $I_{Na/Ca}$ induced by different concentrations of Sr^{2+}. Errors indicate the SEM.

ACKNOWLEDGMENTS

We thank Dr. Alison Obergrussberger, Dr. Markus Rapedius, and Dr. Christian Grimm for proofreading the manuscript, as well as Prof. Jan C. Behrends for supporting this work with microscopic imaging.

This work was supported by funding from the German Research Foundation (SFB/TRR 152 TP06 and SFB 870 TP B05 to C. Wahl-Schott).

The authors M. Barthmes and A. Brüggemann are employed by Nanion Technologies GmbH. There are no limitations regarding the disclosure or use of the data in this work and no patent conflicts. The authors declare no additional competing financial interests.

Merritt Maduke served as editor.

Submitted: 22 February 2016
Accepted: 11 May 2016

REFERENCES

Alexander, S.P.H., H.E. Benson, E. Faccenda, A.J. Pawson, J.L. Sharman, M. Spedding, J.A. Peters, and A.J. Harmar. CGTP Collaborators. 2013. The concise guide to PHARMACOLOGY 2013/14: transporters. *Br. J. Pharmacol.* 170:1706–1796. http://dx.doi.org/10.1111/bph.12450

Angelova, M.I. 2000. Liposome electroformation. In Perspectives in Supramolecular Chemistry: Giant Vesicles. Vol. 6. P.L. Luisi, and P. Walde, editors. John Wiley and Sons, Ltd., Chinchester, UK. 27–37.

Bamberg, E., H.J. Butt, A. Eisenrauch, and K. Fendler. 1993. Charge transport of ion pumps on lipid bilayer membranes. *Q. Rev. Biophys.* 26:1–25. http://dx.doi.org/10.1017/S0033583500003942

Bazzone, A., W.S. Costa, M. Braner, O. Călinescu, L. Hatahet, and K. Fendler. 2013. Introduction to solid supported membrane based electrophysiology. *J. Vis. Exp.* 2013:e50230.

Bers, D.M. 2002. Cardiac excitation-contraction coupling. *Nature.* 415:198–205. http://dx.doi.org/10.1038/415198a

Bers, D.M., C.W. Patton, and R. Nuccitelli. 2010. A practical guide to the preparation of Ca^{2+} buffers. *Methods Cell Biol.* 99:1–26. http://dx.doi.org/10.1016/B978-0-12-374841-6.00001-3

Blaustein, M.P., and W.J. Lederer. 1999. Sodium/calcium exchange: its physiological implications. *Physiol. Rev.* 79:763–854.

Boyman, L., H. Mikhasenko, R. Hiller, and D. Khananshvili. 2009. Kinetic and equilibrium properties of regulatory calcium sensors of NCX1 protein. *J. Biol. Chem.* 284:6185–6193. http://dx.doi.org/10.1074/jbc.M809012200

DeFelice, L.J., and T. Goswami. 2007. Transporters as channels. *Annu. Rev. Physiol.* 69:87–112. http://dx.doi.org/10.1146/annurev.physiol.69.031905.164816

Fendler, K., M. Klingenberg, G. Leblanc, J.J.H.H.M. de Pont, B. Kelety, W. Dörner, and E. Bamberg. 2004. Transport proteins on solid-supported membranes: From basic research to drug discovery. *In* Ultrathin Electrochemical Chemo- and Biosensors. V.M. Mirsky, editor. Springer-Verlag, Berlin. 331–349. http://dx.doi.org/10.1007/978-3-662-05204-4_13

Garcia-Celma, J., A. Szydelko, and R. Dutzler. 2013. Functional characterization of a ClC transporter by solid-supported membrane electrophysiology. *J. Gen. Physiol.* 141:479–491. http://dx.doi.org/10.1085/jgp.201210927

Geibel, S., N. Flores-Herr, T. Licher, and H. Vollert. 2006. Establishment of cell-free electrophysiology for ion transporters: application for pharmacological profiling. *J. Biomol. Screen.* 11:262–268. http://dx.doi.org/10.1177/1087057105285110

Henry, L.K., H. Iwamoto, J.R. Field, K. Kaufmann, E.S. Dawson, M.T. Jacobs, C. Adams, B. Felts, I. Zdravkovic, V. Armstrong, et al. 2011. A conserved asparagine residue in transmembrane segment 1 (TM1) of serotonin transporter dictates chloride-coupled neurotransmitter transport. *J. Biol. Chem.* 286:30823–30836. http://dx.doi.org/10.1074/jbc.M111.250308

Hilgemann, D.W. 1996. Unitary cardiac Na^+, Ca^{2+} exchange current magnitudes determined from channel-like noise and charge movements of ion transport. *Biophys. J.* 71:759–768. http://dx.doi.org/10.1016/S0006-3495(96)79275-5

Holden, M.A., L. Jayasinghe, O. Daltrop, A. Mason, and H. Bayley. 2006. Direct transfer of membrane proteins from bacteria to planar bilayers for rapid screening by single-channel recording. *Nat. Chem. Biol.* 2:314–318. http://dx.doi.org/10.1038/nchembio793

Hsieh, C.H., S.C. Sue, P.C. Lyu, and W.G. Wu. 1997. Membrane packing geometry of diphytanoylphosphatidylcholine is highly sensitive to hydration: phospholipid polymorphism induced by molecular rearrangement in the headgroup region. *Biophys. J.* 73:870–877. http://dx.doi.org/10.1016/S0006-3495(97)78120-7

Iwamoto, T., and M. Shigekawa. 1998. Differential inhibition of Na^+/Ca^{2+} exchanger isoforms by divalent cations and isothiourea derivative. *Am. J. Physiol.* 275:C423–C430.

Kelety, B., K. Diekert, J. Tobien, N. Watzke, W. Dörner, P. Obrdlik, and K. Fendler. 2006. Transporter assays using solid supported membranes: a novel screening platform for drug discovery. *Assay Drug Dev. Technol.* 4:575–582. http://dx.doi.org/10.1089/adt.2006.4.575

Khananshvili, D. 2013. The SLC8 gene family of sodium-calcium exchangers (NCX) - structure, function, and regulation in health and disease. *Mol. Aspects Med.* 34:220–235. http://dx.doi.org/10.1016/j.mam.2012.07.003

Krause, R., N. Watzke, B. Kelety, W. Dörner, and K. Fendler. 2009. An automatic electrophysiological assay for the neuronal glutamate transporter mEAAC1. *J. Neurosci. Methods.* 177:131–141. http://dx.doi.org/10.1016/j.jneumeth.2008.10.005

Kreir, M., C. Farre, M. Beckler, M. George, and N. Fertig. 2008. Rapid screening of membrane protein activity: electrophysiological analysis of OmpF reconstituted in proteoliposomes. *Lab Chip.* 8:587–595. http://dx.doi.org/10.1039/b713982a

Liao, J., H. Li, W. Zeng, D.B. Sauer, R. Belmares, and Y. Jiang. 2012. Structural insight into the ion-exchange mechanism of the sodium/calcium exchanger. *Science.* 335:686–690. http://dx.doi.org/10.1126/science.1215759

Mey, I., M. Stephan, E.K. Schmitt, M.M. Müller, M. Ben Amar, C. Steinem, and A. Janshoff. 2009. Local membrane mechanics of pore-spanning bilayers. *J. Am. Chem. Soc.* 131:7031–7039. http://dx.doi.org/10.1021/ja809165h

Ottolia, M., D.A. Nicoll, and K.D. Philipson. 2009. Roles of two Ca^{2+}-binding domains in regulation of the cardiac Na^+-Ca^{2+} exchanger. *J. Biol. Chem.* 284:32735–32741. http://dx.doi.org/10.1074/jbc.M109.055434

Ottolia, M., N. Torres, J.H.B. Bridge, K.D. Philipson, and J.I. Goldhaber. 2013. Na/Ca exchange and contraction of the heart. *J. Mol. Cell. Cardiol.* 61:28–33. http://dx.doi.org/10.1016/j.yjmcc.2013.06.001

Philipson, K.D., and D.A. Nicoll. 2000. Sodium-calcium exchange: a molecular perspective. *Annu. Rev. Physiol.* 62:111–133. http://dx.doi.org/10.1146/annurev.physiol.62.1.111

Pignataro, G., R. Gala, O. Cuomo, A. Tortiglione, L. Giaccio, P. Castaldo, R. Sirabella, C. Matrone, A. Canitano, S. Amoroso, et al. 2004. Two sodium/calcium exchanger gene products, NCX1 and NCX3, play a major role in the development of permanent focal cerebral ischemia. *Stroke.* 35:2566–2570. (published erratum appears in *Stroke.* 2013. 44:e237–e238) http://dx.doi.org/10.1161/01.STR.0000143730.29964.93

Pintschovius, J., and K. Fendler. 1999. Charge translocation by the Na^+/K^+-ATPase investigated on solid supported membranes: rapid solution exchange with a new technique. *Biophys. J.* 76:814–826. http://dx.doi.org/10.1016/S0006-3495(99)77245-0

Sadafi, F.Z., L. Massai, G. Bartolommei, M.R. Moncelli, L. Messori, and F. Tadini-Buoninsegni. 2014. Anticancer ruthenium(III) complex KP1019 interferes with ATP-dependent Ca^{2+} translocation by sarco-endoplasmic reticulum Ca^{2+}-ATPase (SERCA). *ChemMedChem.* 9:1660–1664.

Seifert, K., K. Fendler, and E. Bamberg. 1993. Charge transport by ion translocating membrane proteins on solid supported membranes. *Biophys. J.* 64:384–391. http://dx.doi.org/10.1016/S0006-3495(93)81379-1

Sharma, V., and D.M. O'Halloran. 2014. Recent structural and functional insights into the family of sodium calcium exchangers. *Genesis.* 52:93–109. http://dx.doi.org/10.1002/dvg.22735

Syeda, R., J.S. Santos, and M. Montal. 2014. Lipid bilayer modules as determinants of K^+ channel gating. *J. Biol. Chem.* 289:4233–4243. http://dx.doi.org/10.1074/jbc.M113.530055

Velamakanni, S., C.H.F. Lau, D.A.P. Gutmann, H. Venter, N.P. Barrera, M.A. Seeger, B. Woebking, D. Matak-Vinkovic, L. Balakrishnan, Y. Yao, et al. 2009. A multidrug ABC transporter with a taste for salt. *PLoS One.* 4:e6137. http://dx.doi.org/10.1371/journal.pone.0006137

Wadiche, J.I., and M.P. Kavanaugh. 1998. Macroscopic and microscopic properties of a cloned glutamate transporter/chloride channel. *J. Neurosci.* 18:7650–7661.

Wright, E.M., D.D.F. Loo, and B.A. Hirayama. 2011. Biology of human sodium glucose transporters. *Physiol. Rev.* 91:733–794. http://dx.doi.org/10.1152/physrev.00055.2009

Yasmann, A., and S. Sukharev. 2015. Properties of diphytanoyl phospholipids at the air-water interface. *Langmuir.* 31:350–357. http://dx.doi.org/10.1021/la503800g